The Effect of Different Implementations of the Weak Temperature Gradient Approximation in Cloud Resolving Models

N. Z. Wong[1], Z. Kuang[1,2]

[1]Department of Earth and Planetary Sciences, Harvard University, Cambridge, MA, USA
[2]John A. Paulson School of Engineering and Applied Sciences, Harvard University, Cambridge, MA, USA

Key Points:

- Different implementations of the Weak Temperature Gradient result in divergent model behaviour in idealized setups
- Divergent model behaviour is caused by different treatment of baroclinic modes

Corresponding author: Nathanael Wong, `nathanaelwong@fas.harvard.edu`

Abstract

The weak-temperature gradient (WTG) approximation has been a popular method used to couple convection in limited-area domain simulations to the large-scale dynamics. Two major implementations that use the WTG approximation have gained popular use over the past two decades - the Temperature Gradient Relaxation implementation and the Damped Gravity Wave implementation. Our comparison of these different WTG implementations in an idealised framework result in different model behaviour, with implications on the nature of convective self-aggregation in similarly idealised setups. A further investigation shows that the different model behaviour is caused by the treatment of the different baroclinic modes by the different WTG implementations. More specifically, we hypothesise that the ratio of the strengths of the baroclinic modes is important in determining if multiple-equilibria states are obtained under different WTG implementations. By varying the strengths of these two baroclinic modes, we are thus able to understand the differences between the WTG schemes.

Plain Language Summary

The Weak-Temperature Gradient (WTG) approximation states that temperature gradients are weak in the tropics. Therefore it can be used to approximate the interaction in the tropics between local convection with local vertical motion and the broader-scale climatology. However, there are different implementations of this approximation, which are broadly similar in many aspects, but have been noted in many previous studies to be different in the details. Although some studies aimed to quantify the differences between the implementations in various models, they did not delve into the reason behind these differences.

We investigated the different model behaviours that result when different WTG implementations are utilized in an idealised model setup. We show through both mathematical analysis of the relevant equations in the WTG implementations, and model runs, that model behaviour under the WTG approximation is dependent on how the different WTG implementations treat the structure of the vertical profiles of temperature and vertical velocity in the atmosphere. If we modify these schemes such that they are able to treat the vertical structure of the atmosphere in a similar manner, many of the differences in model behaviour observed when different WTG schemes are used can therefore be reduced.

1 Introduction

The weak temperature gradient (WTG) approximation (Sobel & Bretherton, 2000) is a simplified framework for atmospheric dynamics in the deep tropics where the Coriolis force is weak. In such a framework, buoyancy gradients in the free troposphere are rapidly smoothed out by gravity waves, and thus spatial and temporal temperature gradients in the free troposphere are small. Local perturbations in buoyancy caused by heating (cooling) are assumed to be balanced by vertical ascent (subsidence). Thus, vertical motion is strongly coupled to convection within the deep tropics, as opposed to it being a one-way, causal, relationship (Raymond & Zeng, 2005). The WTG approximation is therefore a more suitable framework for parameterizing the large-scale circulation in the tropics as opposed to directly specifying the large-scale vertical ascent.

A number of studies (e.g., Raymond & Zeng, 2005; Sobel et al., 2007; Sessions et al., 2010; Daleu et al., 2012; Emanuel et al., 2014; Daleu et al., 2015, and others) have investigated the WTG approximation framework in small-domain Radiative-Convective Equilibrium (RCE) simulations. One common feature found in these studies is that applying the WTG approximation can cause a bifurcation in model equilibrium, resulting in: (1) dry, often non-precipitating states, or (2) heavily-precipitating states. Emanuel

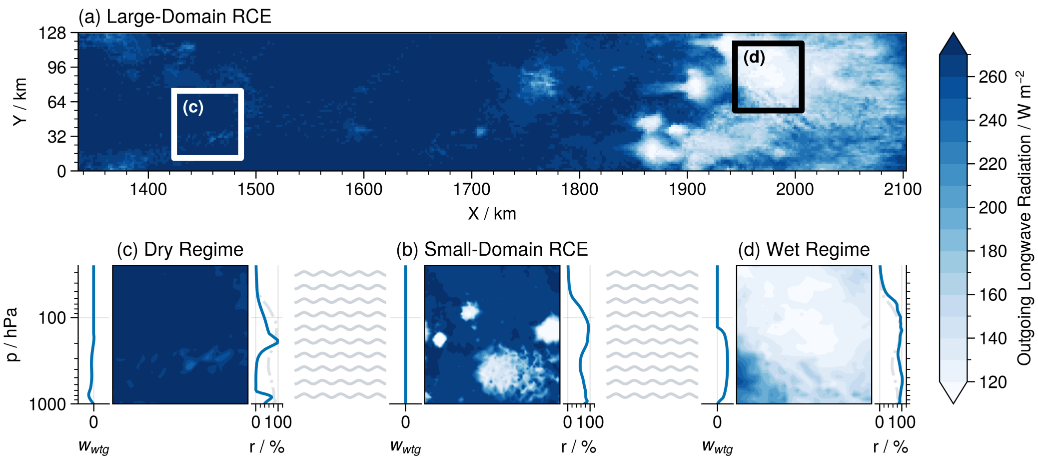

Figure 1. When (a) a large-domain simulation is run to radiative-convective equilibrium, we see that in contrast to a (b) small-domain run, the large-domain simulation will collapse into either (c) a dry, weakly/no-precipitating regime with vertical subsidence or (d) a moist, strongly precipitating regime with vertical ascent. However, using implementations of the weak-temperature gradient approximation, where gravity waves (grey waves) smooth out buoyancy perturbations, previous studies have managed to approximate these two end-regimes with small-domain simulations.

et al. (2014) in particular deduced that these two regimes are actually analogues to the dry and wet regimes of self-aggregation seen in large-domain RCE simulations (Fig. 1a).

Over time, two main implementations have emerged as popular schemes to simulate the WTG approximation in models, the: (1) Temperature Gradient Relaxation (TGR) implementation (Raymond & Zeng, 2005), and the (2) Damped Gravity Wave (DGW) implementation (Kuang, 2008a; Blossey et al., 2009). More elaboration on these schemes is provided in Section 2. Despite the prevalence of these schemes in modelling work for tropical climate, they often produce noticeably different results. For example, it has been repeatedly noted (Romps, 2012b, 2012a; Daleu et al., 2015) that the TGR implementation results in a vertical profile that is noticeably more top-heavy than the DGR implementation.

While some work has gone into quantifying the discrepancies in model results when different implementations are used (Daleu et al., 2015), less thought has been given to understanding why different implementations give rise to different results in the first place. Our study attempts to bridge the gap between the DGW and TGR implementations. In Section 2 we will discuss these two main implementations of the WTG approximation in models, and then show in Section 3 that these two implementations will give markedly different results even in idealized setups. In Section 4, we decompose the model into the first and second baroclinic modes to explain why different implementations give rise to different results, and analyze it in the framework of convectively coupled waves and Gross Moist Stability in Section 5.

2 Weak Temperature Gradient Implementations in Models

Since the WTG approximation was conceptualized by Sobel and Bretherton (2000), there are two major implementations of the WTG that are widely used:

(1) The Temperature Gradient Relaxation (TGR) implementation, which directly calculates large-scale vertical motion from the perturbations in the large-scale potential temperature profile.
(2) The Damped Gravity Wave (DGW) implementation, which uses damped and linearized momentum equations together with the continuity equation and assumptions of hydrostatic balance, to relate the large-scale vertical motion from the perturbations in the large-scale virtual temperature profile.

2.1 The Temperature Gradient Relaxation Implementation

The TGR implementation assumes that the differences in buoyancy between the cloud-resolving model and large-scale environment over a time-scale τ are balanced by the vertical advection of potential temperature $w\partial_z\theta$, such that at a height in the free troposphere z_i the WTG-induced vertical velocity w_{wtg} is given by:

$$w_{\mathrm{wtg}}(z_i)\frac{\partial\overline{\theta}}{\partial z}\bigg|_{z=z_i} = \frac{\overline{\theta}(z_i)-\theta_0(z_i)}{\tau}\cdot\sin\frac{\pi z}{z_t} \tag{1}$$

Where z_t is the height of the tropopause, θ is the model potential temperature, $\overline{\theta}$ is its horizontal average, and θ_0 is the large-scale reference potential temperature. This implementation was first done by Raymond and Zeng (2005), and has become popular due to the straightforward conceptual picture it provides (e.g. Raymond & Zeng, 2005; Sessions et al., 2010; Daleu et al., 2012; Herman & Raymond, 2014). In contrast to Raymond and Zeng (2005) who fixed $z_t = 15$ km, in our runs we allowed z_t to vary by setting it to be the level at which the atmospheric temperature is a minimum, similar to the DGW implementation in SAM as implemented by Blossey et al. (2009). In order to prevent unrealistically large values of w_{wtg}, it is necessary to place a lower-bound on static stability $\partial\overline{\theta}/\partial z$. We set $(\partial\overline{\theta}/\partial z)_{\min} = 1$ K km^{-1} similar to in Raymond and Zeng (2005).

2.2 The Damped Gravity Wave Implementation

At their core, the DGW implementations are based on the damping of gravity waves by the Rayleigh damping coefficient a_m in the momentum equations (2) and (3):

$$u'_t = -\frac{1}{\rho}p'_x + fv - a_m u' \tag{2}$$

$$v'_t = -\frac{1}{\rho}p'_y - fu - a_m v' \tag{3}$$

Using the ideal gas law, hydrostatic balance and mass conservation laws, the momentum equations are thus transformed into the following governing equation for WTG-induced pressure velocity ω_{wtg}:

$$\frac{\partial}{\partial p}\left(\frac{f^2+a_m^2}{a_m}\frac{\partial\omega_{\mathrm{wtg}}}{\partial p}\right) \approx \frac{k^2 R_d}{\overline{p}}T'_v \tag{4}$$

where R_d is the dry gas constant, T_v is the virtual temperature, and k is the horizontal wavenumber of the gravity wave. $(\cdot)'$ represents the perturbation of the variable $(\cdot)$ from the large-scale reference profile. We used Eq. 4 in our experiments, as it was implemented and distributed by Blossey et al. (2009) in the System for Atmospheric Modelling (SAM). Kuang (2008a) also implemented a similar form in SAM using height coordinates instead of pressure coordinates. By setting the Coriolis parameter $f = 0$, which is valid in the deep tropics, we see that Eq. 4 reduces to that of Kuang (2008a). If we further assume that a_m is constant with height, Eq. 4 can be further simplified to:

$$\frac{\partial^2 \omega'}{\partial p^2} = \frac{k^2}{a_m} \frac{R_d T_v'}{\overline{p}} \quad \text{or} \quad \frac{\partial^2 (\rho w')}{\partial z^2} = \frac{k^2}{a_m} \frac{\overline{p} g^2}{R_d \overline{T}^2} T_v' \tag{5}$$

The strength of the implementation is controlled by both a_m and k. Our simplifications ($f = 0$ and $a_m(p)$ is constant) mean that varying either will change model behaviour in a similar manner, so we keep $k = 2\pi/\lambda$ constant, taking $\lambda/4 = 650$ km as in Blossey et al. (2009), and vary a_m.

3 Experimental Setup

3.1 Model Description

We used the System for Atmospheric Modelling (SAM) (Khairoutdinov & Randall, 2003) version 6.10.9 configured in cloud-resolving mode. The model solves the anelastic continuity, momentum, and tracer conservation equations, with total nonprecipitating water (vapor, cloud water, cloud ice) and total precipitating water (rain, snow, graupel) included as prognostic thermodynamic variables. Simulations are run in three dimensions with doubly-periodic boundaries and a horizontal resolution at 4 km to permit clouds. Simulations were also ran at the 2 km resolution, but we found no noticeable differences in the model results. There are 64 vertical levels in our model, with the vertical spacing increasing from 50 m at the boundary layer to around 500 m at the tropical tropopause, to a total height of $\sim$27 km with a rigid upper-bound. Damping is applied to the upper third of the model domain to reduce reflection of gravity waves. A simple Smagorinsky-type scheme is used for the effect of subgrid-scale motion.

In all our experiments, the sea-surface temperature (SST) is fixed at 300 K, spatially uniform and time-invariant. We also assume that there is no coriolis force (i.e. $f = 0$). In place of a full radiative scheme, our idealised model framework uses the fixed radiative-cooling in the troposphere of Pauluis and Garner (2006), with a cooling rate of -1.5 K day^{-1}, and Newtonian relaxation when the temperature is less than 205 K with a relaxation timescale of 5 days. Furthermore, we idealised the surface fluxes by calculating bulk surface-fluxes based on a fixed surface wind speed of 5 m s^{-1}.

3.2 Obtaining the WTG Reference Profile

Our reference large-scale profiles were obtained by spinning a 10-member ensemble in the idealised framework to radiative-convective equilibrium over 2000 days, taking the last 500 days for statistics. We then take the average of the vertical profiles of temperature and specific humidity of these ensemble members to construct a reference large-scale profile. We then take this reference profile and rerun the model to RCE again. This cycle was repeated until the final reference-profiles were deemed to be close to the initial reference profile used to initialise the model runs.

3.3 Implementing the different schemes into SAM

Once the models have been spun-up to RCE, we take the average temperature and humidity vertical profiles of a 10-member ensemble as the large-scale reference profiles. We then apply the WTG approximation schemes to the models over a range of τ or a_m (depending on the WTG scheme used) values, and run a 5-member ensemble over a period of 250 days for each of the configurations, taking statistics every 3 hours over the last 100 days. For each member in the ensembles, perturbations were made to the initial state of the model, resulting in a mix of wet and dry final states. In order to force out both wet- and dry-states of the multiple equilibria, we perturbed the large-scale reference profile uniformly in the vertical by -0.05 K for another 5-member ensemble, and $+0.05$ K for a final 5-member ensemble respectively.

In order to showcase the difference between the RCE and WTG states, we implement a smooth transition from a pseudo-RCE state ($a_m(t = 0) = \tau(t = 0) = \infty$) to a WTG state ($a_m = a_{m.0}$ or $\tau = \tau_0$), where $a_{m.0}$ and τ_0 are the final strength of the WTG approximation at $t = t_{\mathrm{wtg}}$. In this manner, we will be able to better distinguish in between models in RCE and models in WTG in time-series plots. In all our experiments, we take $t_{\mathrm{wtg}} = 50$ days, which means that in our experimental runs the WTG implementations will reach maximum strength at 50 days from model startup.

4 Divergence in Model Behaviour with different WTG Schemes under an Idealised Model Framework

Our implementation of both the TGR and DGW frameworks to small-domain models with interactive radiative and surface-flux schemes results in multiple-equilibria that is consistent the results of Emanuel et al. (2014) using the MITgcm in single-column mode (see Fig. S1). However, in the idealised framework described in Section 3, we see that the model behaviour varies quite markedly between the different schemes. When the DGW implementation is used, as a_m decreases to between 10 and 100 day^{-1} the model first enters the multiple-equilibria regime with noticeable bifurcation between wet and dry states (Fig. 2). As a_m continues to decrease, the model transitions out of this multiple-

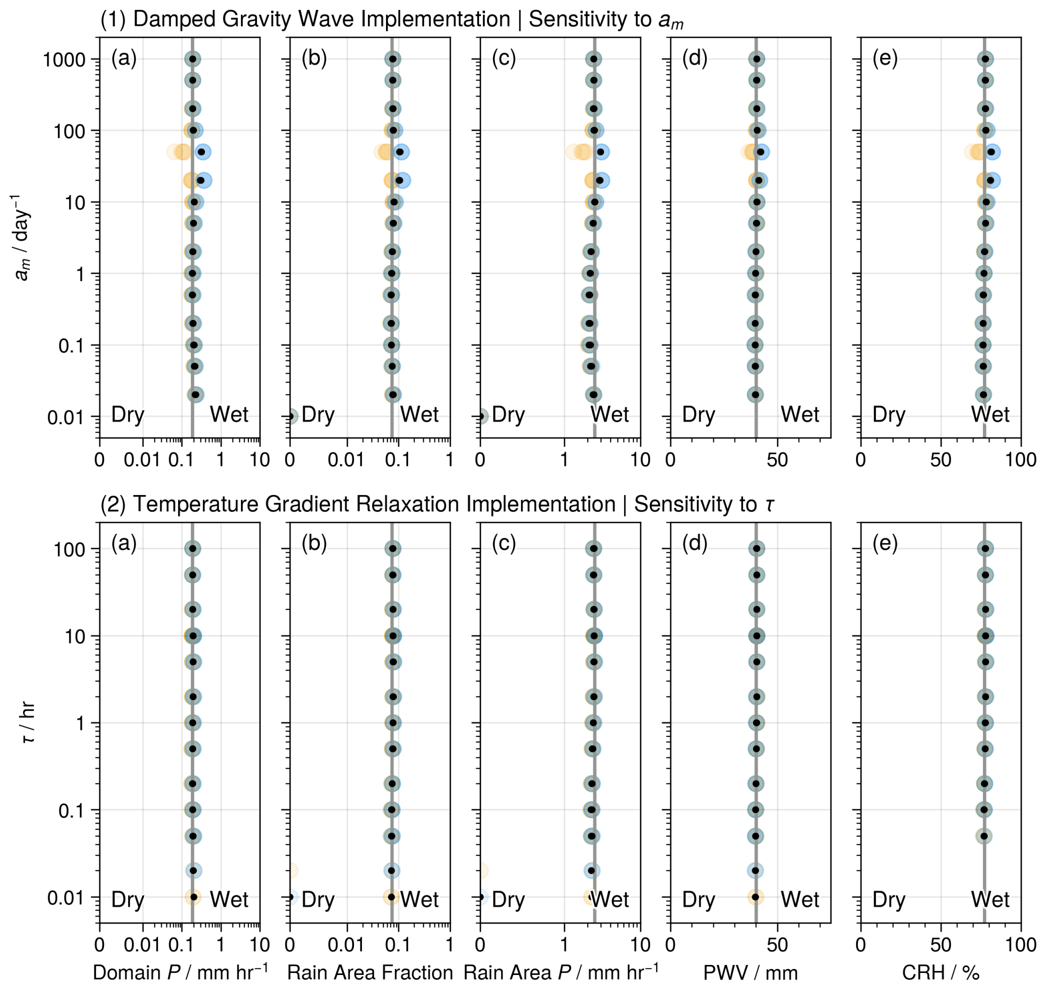

Figure 2. We plot (a) domain-mean precipitation, (b) rain area fraction, (c) rain area precipitation rate, (d) domain-mean precipitatable water vapour and (e) domain-mean column relative humidity that result when the DGW (Kuang, 2008a; Blossey et al., 2009) and TGR (Raymond & Zeng, 2005; Sessions et al., 2010) schemes are implemented with different strengths to three different 5-member small-domain model ensembles. Black dots denote the model ensemble using the default reference profile, yellow dots represent the ensemble results from a reference profile perturbed by +0.05 K at all levels, and blue dots indicate ensemble results from a reference profile perturbed by -0.05 K at all levels.

equilibria regime and the time-averaged domain-mean climatology returns to near-RCE values. Yet, plotting the full time-series shows that the model has not returned to an RCE-equivalent state, but rather oscillates between wet and dry regimes in a manner reminiscent to that of convectively-coupled waves (Fig. 3a,b). However, when the TGR implementation is used, the model transitions directly from an RCE state to an oscillatory state is characteristic of convectively coupled waves as $\tau \to 0$ without displaying multiple-equilibria.

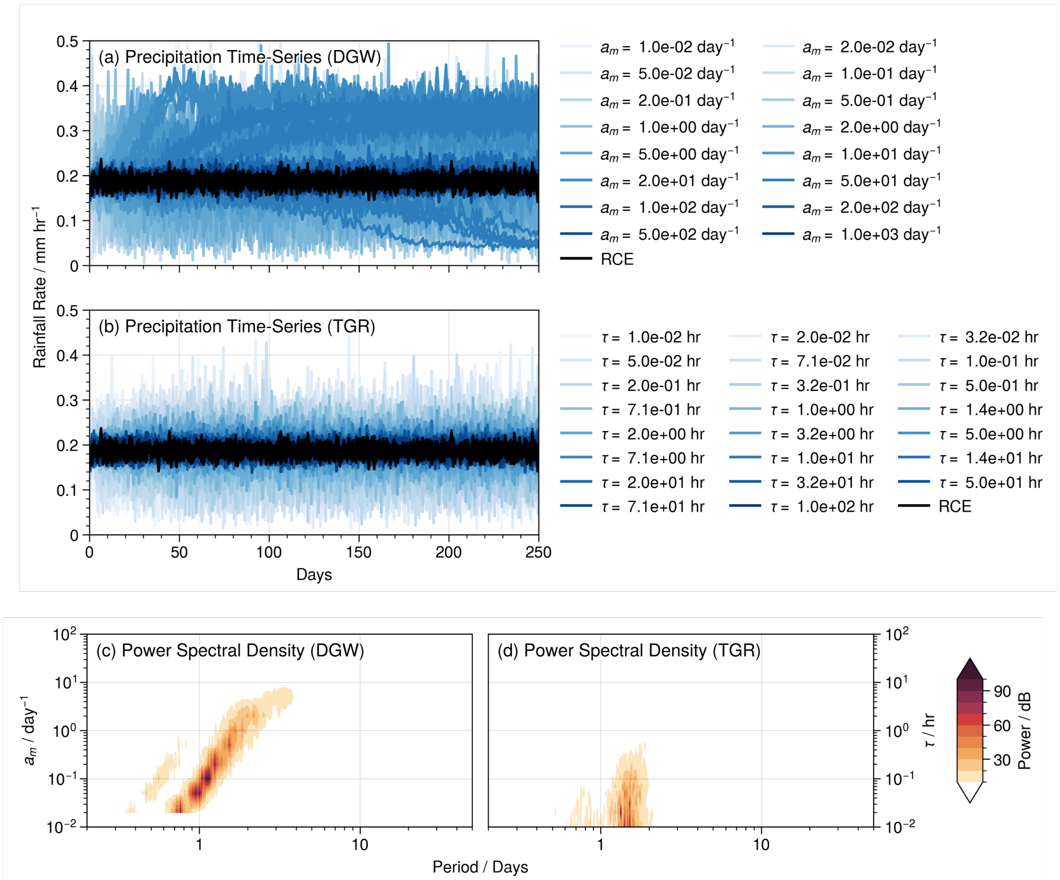

Figure 3. We plot the daily time-series of precipitation for the (a) DGW and (b) TGR implementations of varying strengths. We see that while in Fig. 2 the time-average is close to RCE, the time-series shows that the model actually fluctuates between wet and dry regimes in a manner similar to convectively coupled wave behaviour. Furthermore, we also plot the power spectrum for the timeseries in (c) and (d) respectively, where we see that rough analogues of convectively coupled waves appear when the implementation strength is great enough.

Furthermore, the power spectrum of the time-series (Fig. 3c,d) indicates that the nature of the wet-dry oscillation is also different. When the TGR implementation is used, the oscillatory frequency seems to remain constant as the relaxation timescale τ decreases, but when the DGW implementation is used, the frequency decreases approximately linearly with decreasing a_m. We do see that for both the DGW and TGR implementations, the amplitude of the oscillations reaches a maximum point at a certain value (between $a_m = 0.1$-0.05 day^{-1} and $\tau = 0.01$-0.02 hr) and decreases away from it. The disparate model behaviour that results when different WTG implementations are used, even in this idealised framework, indicates that there are significant differences between them.

As both these WTG schemes are widely used, it is important for us to understand the differences between these implementations. We begin by recalling previous studies which have shown that the basic dynamics of convectively coupled tropical waves can largely be captured by models which contain the first two baroclinic modes of the vertical structure of the tropical atmosphere (e.g. Mapes, 2000; Majda & Shefter, 2001; Khouider & Majda, 2006; Haertel & Kiladis, 2004; Kuang, 2008b). Similar to (Kuang, 2008b), we expand both the vertical velocity and temperature perturbation components of Raymond and Zeng (2005) in terms of the first two vertical eigenmodes G_j:

$$w' = \frac{\theta'}{\tau \cdot \partial_z \overline{\theta}} \qquad \frac{\partial^2 \omega'}{\partial z^2} = \frac{k^2}{a_m} \frac{\overline{p} g^2}{R_d \overline{T}^2} T_v' \tag{6}$$

$$w' = \sum_{j=1}^{2} w_j G_j(z) \qquad \omega' = \sum_{j=1}^{2} \omega_j G_j(z) \tag{7}$$

$$\frac{\theta'}{\partial_z \overline{\theta}} = \sum_{j=1}^{2} \theta_j G_j(z) \qquad \frac{\overline{p} T_v'}{\overline{T}^2} = \sum_{j=1}^{2} T_j G_j(z) \tag{8}$$

where the vertical modes are of the form:

$$G_j(z) = \frac{\pi}{2} \sin\left(\frac{j\pi z}{z_t}\right) \tag{9}$$

Here, z_t is the height of the troposphere. Note that in Eq. (7), $\omega' = \sum_{j=1}^{2} \omega_j G_j(z)$, but the equations in the DGW implementation solve not for ω', but for $\partial_{zz}\omega'$. Therefore, we see that

$$\partial_{zz}\omega' = -\frac{z_t^2}{\pi^2} \sum_{j=1}^{2} j^2 \omega_j G_j(z) \tag{10}$$

Because j^2 increases with higher-order baroclinic modes, it follows that the amplitude of higher-order baroclinic modes of vertical velocity in the DGW implementation is proportionally weaker for temperature perturbations of the same amplitude. This means that the vertical structure of vertical velocity will be different across the different WTG implementations. The first baroclinic mode of vertical velocity is likely to be stronger than the second baroclinic mode in the DGW implementation, compared to if the TGR implementation is used.

We therefore conclude that vertical profiles resulting from the TGR implementation are likely to be more top- or bottom-heavy compared to the profiles resulting from the DGW implementation. Indeed, the top-heavy nature of vertical profiles of vertical velocities in modelling studies using the TGR implementation has been well-documented (Romps, 2012b; Daleu et al., 2015). We further hypothesize that the strength of this second baroclinic mode relative to the first baroclinic mode is critical in determining the presence of a multiple-equilibria regime when the model is coupled to the WTG schemes.

To test this hypothesis, we modified both of the WTG schemes and calculated the WTG-induced vertical velocities for the TGR and DGW implementations respectively to be:

$$\omega' = c_1 \omega_1 \sin\frac{\pi z}{z_t} + c_2 4\omega_2 \sin\frac{2\pi z}{z_t} \qquad w' = c_1 w_1 \sin\frac{\pi z}{z_t} + c_2 w_2 \sin\frac{2\pi z}{z_t} \tag{11}$$

where c_1 and c_2 vary the strength of the response of the first and second baroclinic modes of the vertical velocity to the first and second baroclinic modes of the temperature perturbation. The constant factor of 4 in front of ω_2 ensures that the ratios of the first and second baroclinic modes are the same across the induced vertical velocity and temperature perturbation.

We vary different configurations of c_1 and c_2 as follows:

$$(c_1, c_2) = \begin{cases} 0 \leq c_1 \leq 1 & c_2 = 1 \\ 0 \leq c_2 \leq 1 & c_1 = 1 \end{cases} \tag{12}$$

We then plot the results below for $a_m = 10$ day^{-1} and $\tau = 10$ hr (Fig. 4). We see that the presence and strength of multiple-equilibria is tied to the ratio of $c_r = c_2/c_1$, with smaller values of c_r resulting in stronger bifurcation between the wet and dry equilibrium states. When $c_2 = 0$ (i.e. when only the first baroclinic mode is allowed to respond), the model is unable to force out a dry regime. Alternatively, when $c_1 = 0$, there is no bifurcation between wet and dry equilibrium states, and an analysis of the time-series (not shown) shows no distinction between the model to the 2-day wave behaviour, even at much lower values of τ. Although the change in magnitude of the bifurcation is quantitatively different, this can be attributed to the fact that the TGR and DGW implementations solve for the pressure velocity and vertical velocity respectively, and these two variables are not precisely the same.

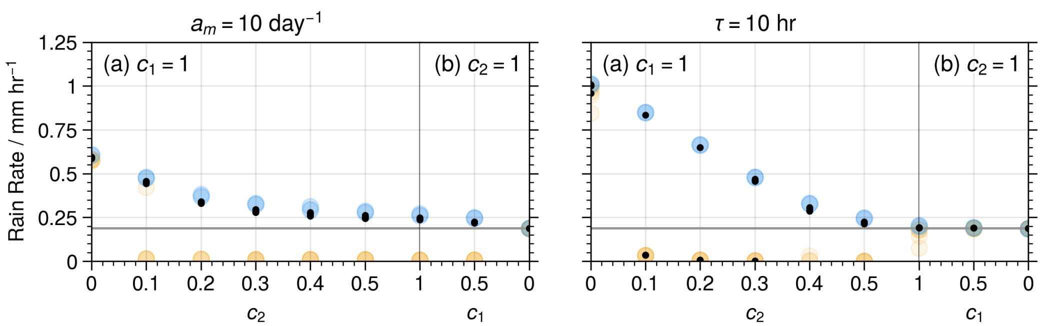

Figure 4. We plot the daily time-series of precipitation for the (a) DGW and (b) TGR implementations of varying strengths. We see that while in Fig. 2 the time-average is close to RCE, the time-series shows that the model actually fluctuates between wet and dry regimes in a manner similar to the 2-day wave behaviour of Takayabu et al. (1996). Furthermore, we also plot the power spectrum for the timeseries in (c) and (d) respectively, where we see that rough analogues of this 2-day wave behaviour appear when the implementation strength is great enough.

5 Bringing the different WTG Schemes together

We analyze both WTG implementations in the framework of Gross Moist Stability (Inoue & Back, 2015, 2017), which we define in this instance to be:

$$\text{GMS} = \frac{\langle w \cdot \partial_z h \rangle}{\langle w \cdot \partial_z s \rangle} = \frac{\langle w_H \cdot \partial_z h \rangle + \langle w_F \cdot \partial_z h \rangle}{\langle w_H \cdot \partial_z s \rangle + \langle w_F \cdot \partial_z s \rangle} \tag{13}$$

This is the ratio of the vertical export of moist static energy h to the vertical export of dry static energy s. w_H and w_F are the first and second baroclinic modes of vertical velocity. Taking idealised vertical profiles of the dry and moist static energies shown in Fig. 5, we see that Eq. 13 can be reduced to:

$$\text{GMS} = \frac{\langle w \cdot \partial_z h \rangle}{\langle w \cdot \partial_z s \rangle} \approx \frac{\langle w_F \cdot \partial_z h \rangle}{\langle w_H \cdot \partial_z s \rangle} = \frac{w_2 \langle \sin(2\pi z/z_t) \cdot \partial_z h \rangle}{w_1 \langle \sin(\pi z/z_t) \cdot \partial_z s \rangle} \tag{14}$$

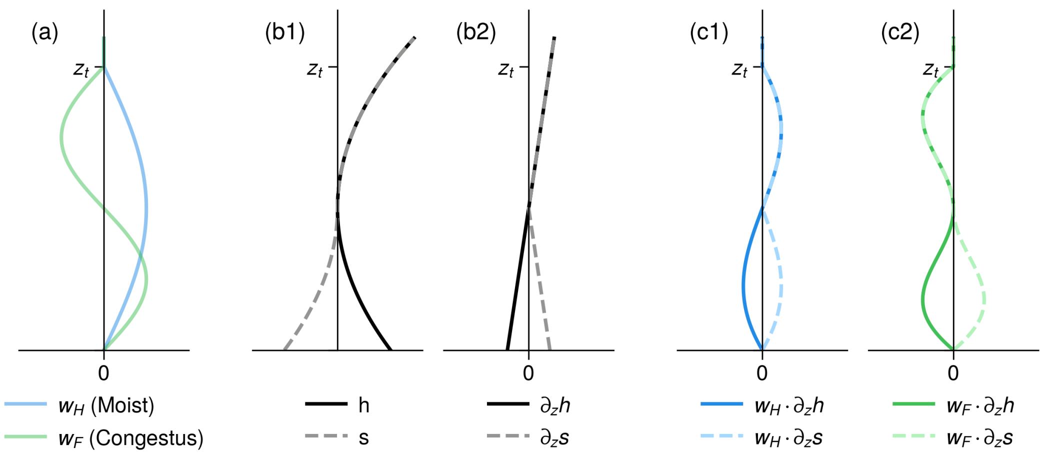

Figure 5. We plot an idealized profile of the (a) first two baroclinic modes of WTG-induced vertical velocity, (b) vertical profiles of (1) dry and moist static energy and (2) their vertical derivatives, and lastly (c) the product of the vertical derivatives of the static energys with the (1) first and (2) second baroclinic modes. We see that the vertical export of moist and dry static energies are dominated by the 2nd and 1st baroclinic modes respectively.

We therefore see that any change to the Gross Moist Stability is ultimately dominated by the ratio of the baroclinic modes of the WTG-induced vertical velocity. However, as we have discussed in Section 4 the ratio of strengths between the baroclinic modes is different across the WTG implementations. For example, because the TGR implementation results in vertical velocity profiles that have larger 2nd baroclinic modes, it would favour higher GMS magnitudes than the DGW implementation and thus larger magnitudes of vertical export (or import) of moist static energy. This is in line with more recent characterisations of Gross Moist Stability as a quantity that describes the (de)stabilisation mechanisms of convective disturbances in the atmosphere (Inoue & Back, 2015, 2017). We believe that the ratio w_2/w_1 therefore constrains how rapidly these convective disturbances are magnified/reduced.

For example, when w_2/w_1 is small, the impact of w_2 on the convective disturbances represented by w_1 is small. This results in the persistence of these convective disturbances and allows for sustained bifurcation of wet and dry multiple-equilibria states we see in $a_m \sim$ 20-50 day^{-1}. However, when w_2/w_1 is moderate in nature, these perturbations are large enough to impact the convective disturbances, while small enough to allow these disturbances room to grow, causing noticeable oscillatory behaviour between wet- and dry-states that are reminiscent of convectively-coupled waves. Conversely, when w_2/w_1 is large, the growth of these potential convective disturbances, and thus the oscillatory behaviour that is characteristic of convectively coupled waves, is small.

We therefore believe that the discrepancies in model behaviour when different WTG schemes are used can be attributed to the differences in treatment of the baroclinic modes between the two schemes. If we modify the TGR implementation such that the response strength of higher baroclinic modes is reduced, the multiple-equilibria regime appears. Furthermore, as the strength of the WTG implementations increase we see that the model in both schemes tend to converge towards the oscillatory behaviour that is reminiscent of convectively-coupled waves, even if the paths they take to reach this state are different.

6 Conclusions

Implementing different WTG implementations results in different model behaviour even in an simplified framework with idealised radiation and surface-flux schemes. A multiple-equilibria regime appears when the DGW scheme is implemented with consistently wet and dry states. As the strength the implementation increases, the model then transitions into a regime that oscillates between these wet and dry states in a behaviour that is reminiscent of convectively coupled waves. However, when the TGR scheme is implemented we see that there is no multiple-equilibria regime, and the convectively-coupled wave behaviour only appears when the relaxation occurs over unrealistically short timescales ($\tau \sim$ 5 min).

We have shown that these discrepancies in model behaviour to different WTG implementations even in this idealised framework can be attributed to their different treatments of the vertical baroclinic modes. Specifically, we postulate that the TGR scheme overemphasises higher-order vertical modes. By replacing each of the WTG schemes with equivalent models for the first two baroclinic modes (Eq. 11), we see that when the second baroclinic mode is stronger relative to the first baroclinic mode, the degree of bifurcation between the wet- and dry-states in the multiple-equilibria regime decreases.

Lastly, we can understand these differences in the framework of Gross Moist Stability (GMS), specifically in reference to how Inoue and Back (2017) characterized the GMS as a measure of feedback effects to convection. By approximating GMS as the ratio of export of moist static energy to that of dry static energy (Eq. 14, see also Inoue and Back (2015)), we see that the choice of WTG implementation used will play a significant role in the GMS of the system, particularly because the response of the 2nd baroclinic mode of vertical velocity to the 2nd baroclinic mode of the temperature perturbations are treated differently. Thus when the DGW implementation is used in our idealized model setup, the smaller 2nd baroclinic mode in vertical velocity will lead to a smaller GMS response in the system, which gives rise to a measure of stability in the convective states seen in the multiple-equilibria regime, which in contrast is entirely absent when the TGR implementation is chosen.

As we first touched upon in our introduction, while some work has gone into quantifying the discrepancies in model results when different implementations are used (e.g. Daleu et al., 2015), less thought has been given to understanding why different implementations give rise to different results in the first place. We hope that this set of idealized model experiments begins to close the gap between quantifying and understanding the differences in model results when different WTG impleentations are used.

7 Open Research

The model code used is built upon a modified version of Marat Khairoutdinov' System of Atmospheric Modelling (Khairoutdinov & Randall, 2003) by Peter Blossey as in Blossey et al. (2009). Our modified version of the source code for the model is available at `https://github.com/KuangLab-Harvard/SAM_SRCv6.10` and is meant to replace the `SRC` folder of SAM v6.10.6.

The Julia Language code that was used in setting up the model experiments, analyzing our results, and the notebooks used in producing our figures, available at:

```
@software{nathanael_wong_2023_7903686,
  author       = {Nathanael Wong},
  title        = {natgeo-wong/2023GL104350: v0.1},
  month        = may,
  year         = 2023,
  publisher    = {Zenodo},
  version      = {v0.1},
  doi          = {10.5281/zenodo.7903686},
  url          = {https://doi.org/10.5281/zenodo.7903686}
}
```

The raw data used in this paper is available at:

```
@data{DVN/YPXNPG_2023,
    author = {Wong, Nathanael},
    publisher = {Harvard Dataverse},
    title = {{Dataset for ‘‘The Effect of Different Implementations of the Weak Temperature Gradien
    year = {2023},
    version = {V1},
    doi = {10.7910/DVN/YPXNPG},
    url = {https://doi.org/10.7910/DVN/YPXNPG}
}
```

Acknowledgments

This research was supported by NSF grants AGS-1759255 and OISE-1743753. We thank Marat Khairoutdinov for making SAM available. The Harvard Odyssey cluster provided the computing resources for this work.

References

Blossey, P. N., Bretherton, C. S., & Wyant, M. C. (2009, 3). Subtropical Low Cloud Response to a Warmer Climate in a Superparameterized Climate Model. Part II: Column Modeling with a Cloud Resolving Model. *Journal of Advances in Modeling Earth Systems*, *1*(3), n/a-n/a. Retrieved from `http://doi.wiley.com/10.3894/JAMES.2009.1.8` doi: 10.3894/JAMES.2009.1.8

Daleu, C. L., Plant, R. S., Woolnough, S. J., Sessions, S., Herman, M. J., Sobel, A., ... van Ulft, L. (2015, 12). Intercomparison of methods of coupling between convection and large-scale circulation: 1. Comparison over uniform surface conditions. *Journal of Advances in Modeling Earth Systems*, *7*(4), 1576–1601. Retrieved from `http://doi.wiley.com/10.1002/2015MS000468` doi: 10.1002/2015MS000468

Daleu, C. L., Woolnough, S. J., & Plant, R. S. (2012, 12). Cloud-Resolving Model Simulations with One- and Two-Way Couplings via the Weak Temperature Gradient Approximation. *Journal of the Atmospheric Sciences*, *69*(12), 3683–3699. Retrieved from `https://journals.ametsoc.org/doi/10.1175/JAS-D-12-058.1` doi: 10.1175/JAS-D-12-058.1

Emanuel, K., Wing, A. A., & Vincent, E. M. (2014, 3). Radiative-convective instability. *Journal of Advances in Modeling Earth Systems*, *6*(1), 75–90. Retrieved from `http://doi.wiley.com/10.1002/2013MS000270` doi: 10.1002/2013MS000270

Haertel, P. T., & Kiladis, G. N. (2004, 11). Dynamics of 2-Day Equatorial Waves. *Journal of the Atmospheric Sciences*, *61*(22), 2707–2721. doi: 10.1175/JAS3352.1

Herman, M. J., & Raymond, D. J. (2014, 12). WTG cloud modeling with spectral decomposition of heating. *Journal of Advances in Modeling Earth Systems*, *6*(4), 1121–1140. Retrieved from `http://doi.wiley.com/10.1002/2014MS000359` doi: 10.1002/2014MS000359

Inoue, K., & Back, L. E. (2015, 11). Gross Moist Stability Assessment during TOGA COARE: Various Interpretations of Gross Moist Stability. *Journal of the Atmospheric Sciences*, *72*(11), 4148–4166. doi: 10.1175/JAS-D-15-0092.1

Inoue, K., & Back, L. E. (2017, 6). Gross Moist Stability Analysis: Assessment of Satellite-Based Products in the GMS Plane. *Journal of the Atmospheric Sciences*, *74*(6), 1819–1837. doi: 10.1175/JAS-D-16-0218.1

Khairoutdinov, M. F., & Randall, D. A. (2003, 2). Cloud Resolving Modeling of the ARM Summer 1997 IOP: Model Formulation, Results, Uncertainties, and Sensitivities. *Journal of the Atmospheric Sciences*, *60*(4), 607–625. Retrieved from `http://journals.ametsoc.org/doi/abs/10.1175/1520-0469%282003%29060%3C0607%3ACRMOTA%3E2.0.CO%3B2` doi: 10.1175/1520-0469(2003)060⟨0607:CRMOTA⟩2.0.CO;2

Khouider, B., & Majda, A. J. (2006, 4). A Simple Multicloud Parameterization for Convectively Coupled Tropical Waves. Part I: Linear Analysis. *Journal of the Atmospheric Sciences*, *63*(4), 1308–1323. doi: 10.1175/JAS3677.1

Kuang, Z. (2008a, 2). Modeling the Interaction between Cumulus Convection and Linear Gravity Waves Using a Limited-Domain Cloud System–Resolving Model. *Journal of the Atmospheric Sciences*, *65*(2), 576–591. Retrieved from `https://journals.ametsoc.org/doi/10.1175/2007JAS2399.1` doi: 10.1175/2007JAS2399.1

Kuang, Z. (2008b, 3). A Moisture-Stratiform Instability for Convectively Coupled Waves. *Journal of the Atmospheric Sciences*, *65*(3), 834–854. doi: 10.1175/2007JAS2444.1

Majda, A. J., & Shefter, M. G. (2001, 6). Models for Stratiform Instability and Convectively Coupled Waves. *Journal of the Atmospheric Sciences*, *58*(12), 1567–1584. doi: 10.1175/1520-0469(2001)058⟨1567:MFSIAC⟩2.0.CO;2

Mapes, B. E. (2000, 5). Convective Inhibition, Subgrid-Scale Triggering Energy, and Stratiform Instability in a Toy Tropical Wave Model. *Journal of the Atmospheric Sciences*, *57*(10), 1515–1535. doi: 10.1175/1520-0469(2000)057⟨1515:CISSTE⟩2.0.CO;2

Pauluis, O., & Garner, S. (2006, 7). Sensitivity of Radiative–Convective Equilibrium Simulations to Horizontal Resolution. *Journal of the Atmospheric Sciences*, *63*(7), 1910–1923. Retrieved from `https://journals.ametsoc.org/doi/10.1175/JAS3705.1` doi: 10.1175/JAS3705.1

Raymond, D. J., & Zeng, X. (2005, 4). Modelling tropical atmospheric convection in the context of the weak temperature gradient approximation. *Quarterly Journal of the Royal Meteorological Society*, *131*(608), 1301–1320. Retrieved from `http://doi.wiley.com/10.1256/qj.03.97` doi: 10.1256/qj.03.97

Romps, D. M. (2012a, 9). Numerical Tests of the Weak Pressure Gradient Approximation. *Journal of the Atmospheric Sciences*, *69*(9), 2846–2856. Retrieved from `https://journals.ametsoc.org/doi/10.1175/JAS-D-11-0337.1` doi: 10.1175/JAS-D-11-0337.1

Romps, D. M. (2012b, 9). Weak Pressure Gradient Approximation and Its Analytical Solutions. *Journal of the Atmospheric Sciences*, *69*(9), 2835–2845. Retrieved from `https://journals.ametsoc.org/doi/10.1175/JAS-D-11-0336.1` doi: 10.1175/JAS-D-11-0336.1

Sessions, S. L., Sugaya, S., Raymond, D. J., & Sobel, A. H. (2010, 6). Multiple equilibria in a cloud-resolving model using the weak temperature gradient approximation. *Journal of Geophysical Research*, *115*(D12), D12110. Retrieved from `http://doi.wiley.com/10.1029/2009JD013376` doi: 10.1029/2009JD013376

Sobel, A. H., Bellon, G., & Bacmeister, J. (2007, 11). Multiple equilibria in a single-column model of the tropical atmosphere. *Geophysical Research Letters*, *34*(22), L22804. Retrieved from `http://doi.wiley.com/10.1029/2007GL031320` doi: 10.1029/2007GL031320

Sobel, A. H., & Bretherton, C. S. (2000, 12). Modeling Tropical Precipitation in a Single Column. *Journal of Climate*, *13*(24), 4378–4392. Retrieved from `http://journals.ametsoc.org/doi/abs/10.1175/1520-0442%282000%29013%3C4378%3AMTPIAS%3E2.0.CO%3B2` doi: 10.1175/1520-0442(2000)013⟨4378:MTPIAS⟩2.0.CO;2

Takayabu, Y. N., Lau, K.-M., & Sui, C.-H. (1996, 9). Observation of a Quasi-2-Day Wave during TOGA COARE. *Monthly Weather Review*, *124*(9), 1892–1913. doi: 10.1175/1520-0493(1996)124⟨1892:OOAQDW⟩2.0.CO;2

Figure 1.

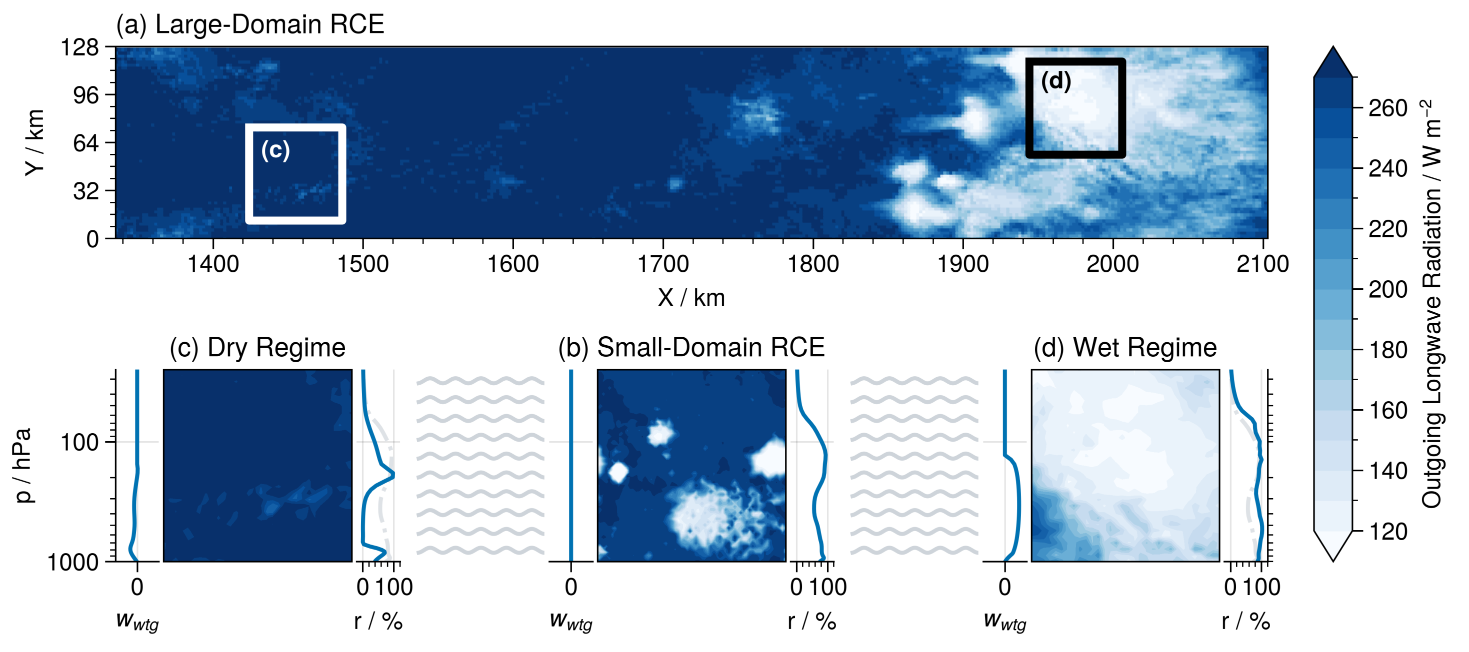
(a) Large-Domain RCE
Y / km
128
96
64
32
0
(c)
(d)
1400
1500
1600
1700
1800
1900
2000
2100
X / km
(c) Dry Regime
(b) Small-Domain RCE
(d) Wet Regime
p / hPa
100
1000
0
0 100
w_{wtg}
r / %
Outgoing Longwave Radiation / W m^{-2}
260
240
220
200
180
160
140
120

Figure 2.

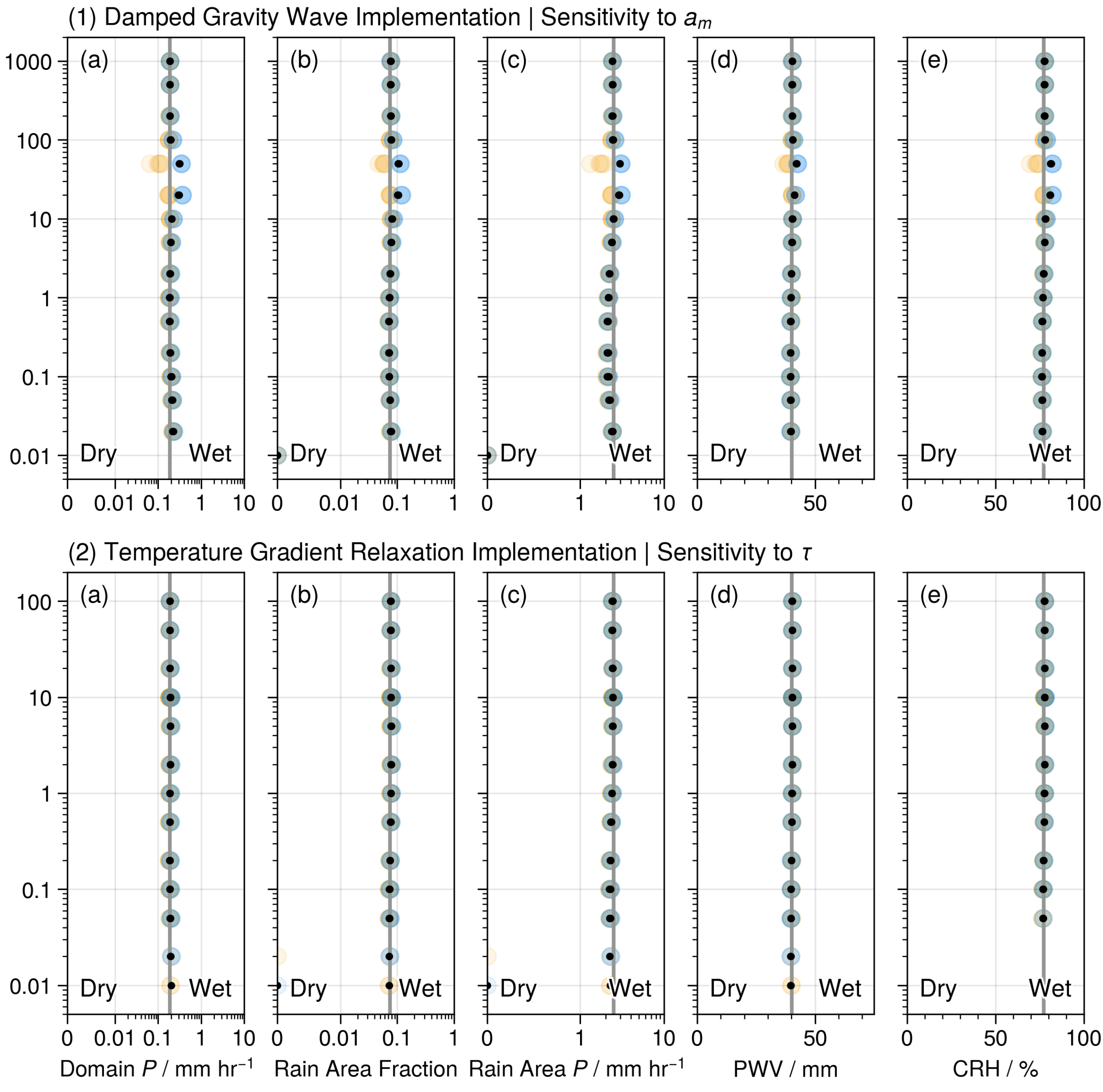

(1) Damped Gravity Wave Implementation | Sensitivity to a_m
(a)
(b)
(c)
(d)
(e)
Dry
Wet
a_m / day^{-1}
1000
100
10
1
0.1
0.01
0
0.01
0.1
1
10
50
100
(2) Temperature Gradient Relaxation Implementation | Sensitivity to τ
τ / hr
Domain P / mm hr^{-1}
Rain Area Fraction
Rain Area P / mm hr^{-1}
PWV / mm
CRH / %

Figure 3.

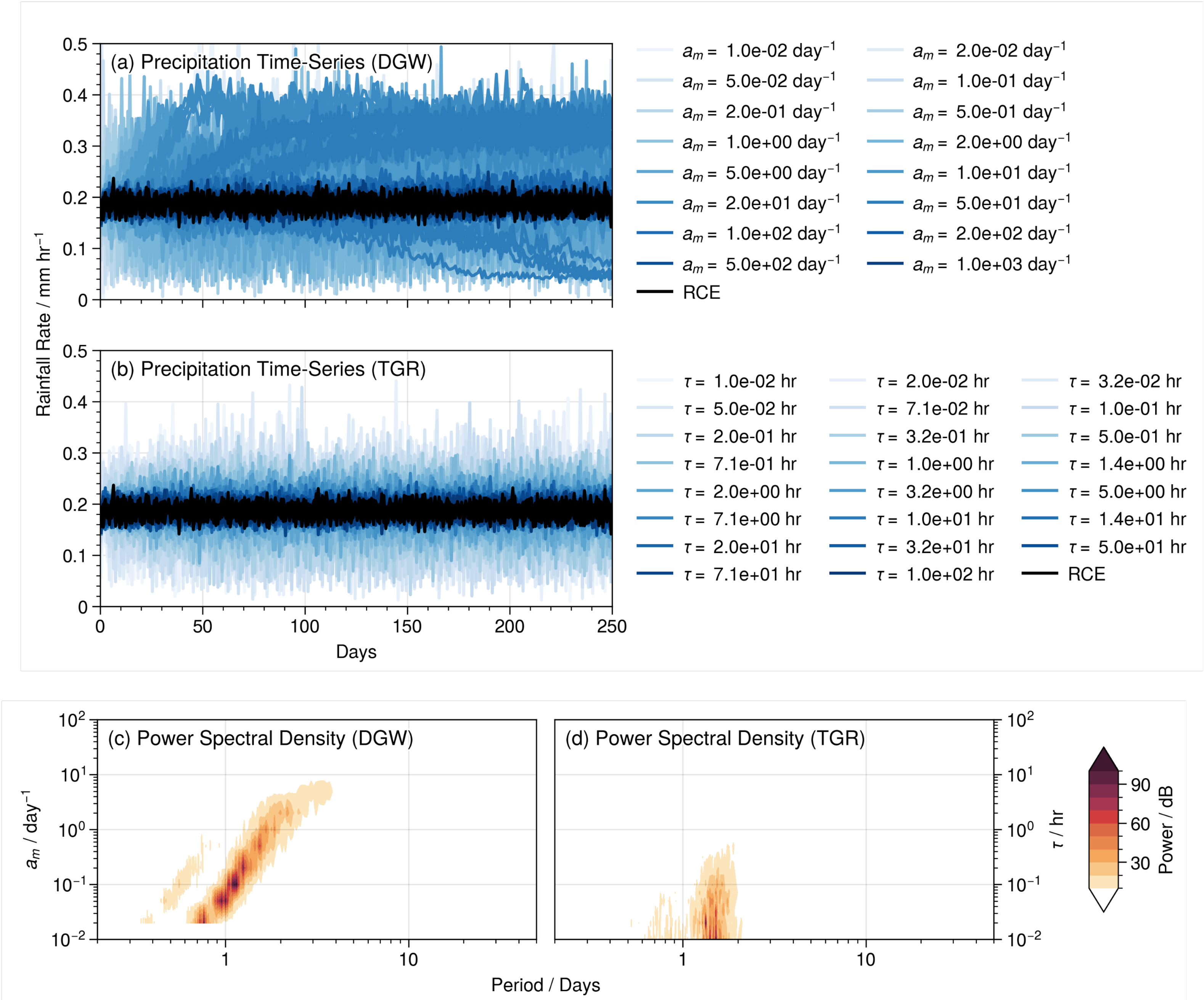

(a) Precipitation Time-Series (DGW)
(b) Precipitation Time-Series (TGR)
Rainfall Rate / mm hr^{-1}
Days
a_m = 1.0e-02 day^{-1}
a_m = 2.0e-02 day^{-1}
a_m = 5.0e-02 day^{-1}
a_m = 1.0e-01 day^{-1}
a_m = 2.0e-01 day^{-1}
a_m = 5.0e-01 day^{-1}
a_m = 1.0e+00 day^{-1}
a_m = 2.0e+00 day^{-1}
a_m = 5.0e+00 day^{-1}
a_m = 1.0e+01 day^{-1}
a_m = 2.0e+01 day^{-1}
a_m = 5.0e+01 day^{-1}
a_m = 1.0e+02 day^{-1}
a_m = 2.0e+02 day^{-1}
a_m = 5.0e+02 day^{-1}
a_m = 1.0e+03 day^{-1}
RCE
τ = 1.0e-02 hr
τ = 2.0e-02 hr
τ = 3.2e-02 hr
τ = 5.0e-02 hr
τ = 7.1e-02 hr
τ = 1.0e-01 hr
τ = 2.0e-01 hr
τ = 3.2e-01 hr
τ = 5.0e-01 hr
τ = 7.1e-01 hr
τ = 1.0e+00 hr
τ = 1.4e+00 hr
τ = 2.0e+00 hr
τ = 3.2e+00 hr
τ = 5.0e+00 hr
τ = 7.1e+00 hr
τ = 1.0e+01 hr
τ = 1.4e+01 hr
τ = 2.0e+01 hr
τ = 3.2e+01 hr
τ = 5.0e+01 hr
τ = 7.1e+01 hr
τ = 1.0e+02 hr
RCE
(c) Power Spectral Density (DGW)
(d) Power Spectral Density (TGR)
a_m / day^{-1}
τ / hr
Period / Days
Power / dB

Figure 4.

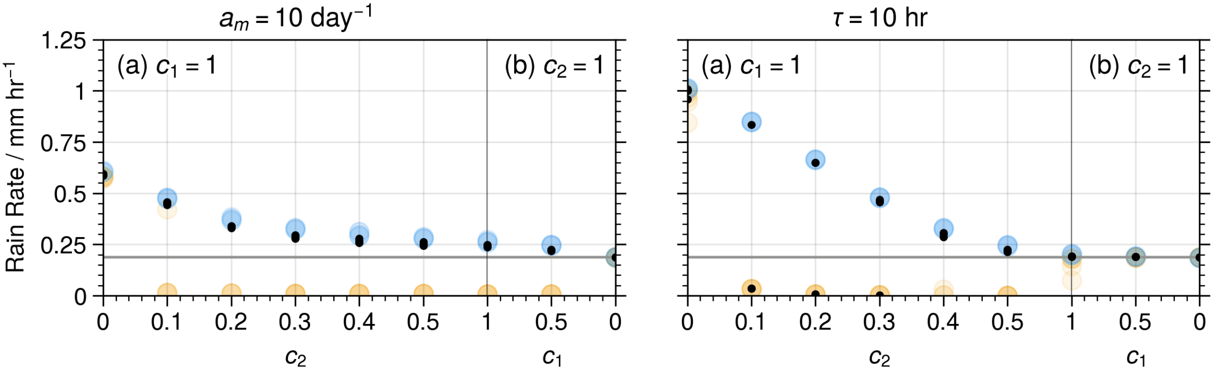

$a_m = 10\ \mathrm{day}^{-1}$
$\tau = 10$ hr
Rain Rate / mm hr^{-1}
(a) $c_1 = 1$
(b) $c_2 = 1$
1.25
1
0.75
0.5
0.25
0
0.1
0.2
0.3
0.4
0.5
c_2
c_1

Figure 5.

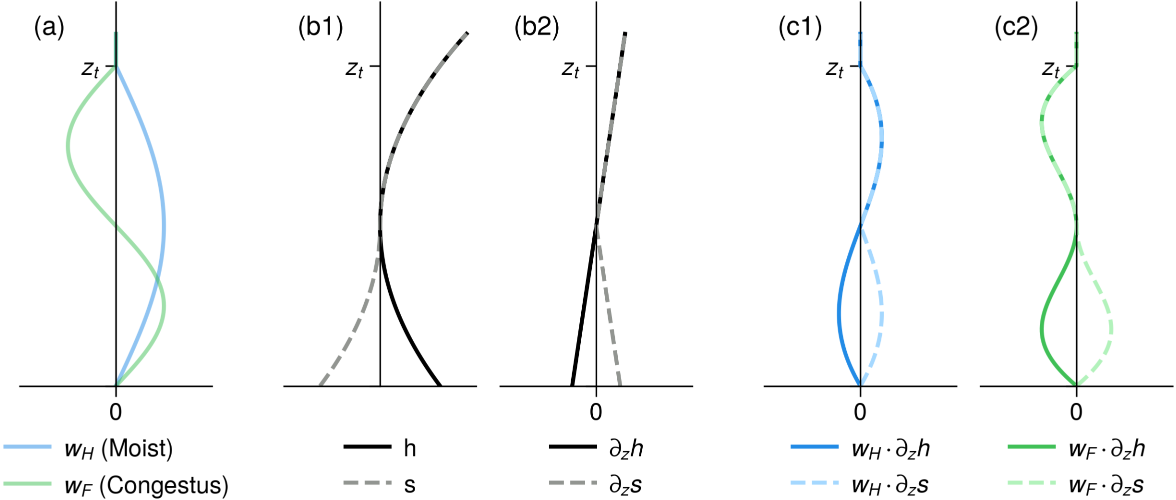

(a)
(b1)
(b2)
(c1)
(c2)
z_t
0
w_H (Moist)
w_F (Congestus)
h
s
$\partial_z h$
$\partial_z s$
$w_H \cdot \partial_z h$
$w_H \cdot \partial_z s$
$w_F \cdot \partial_z h$
$w_F \cdot \partial_z s$